Available online at www.sciencedirect.com
SCIENCE DIRECT®
Journal of Solid State Chemistry 179 (2006) 563–572
JOURNAL OF SOLID STATE CHEMISTRY
www.elsevier.com/locate/jssc

Synthesis, structure and physical properties of Ru ferrites: $BaMRu_5O_{11}$ (M = Li and Cu) and $BaM'_2Ru_4O_{11}$ (M' = Mn, Fe and Co)

M.L. Foo[a,*,1], Q. Huang[b], J.W. Lynn[b], Wei-Li Lee[c], Tomasz Klimczuk[a,d], I.S. Hagemann[a,2], N.P. Ong[c], R.J. Cava[a]

[a]Department of Chemistry, Princeton University, Princeton, NJ 08540, USA
[b]NIST Center for Neutron Research, NIST, Gaithersburg, MD 20899, USA
[c]Department of Physics, Princeton University, Princeton, NJ 08540, USA
[d]Faculty of Applied Physics and Mathematics, Gdansk University of Technology, Narutowicza 11/12, 80-952 Gdansk, Poland

Received 24 August 2005; received in revised form 24 October 2005; accepted 13 November 2005
Available online 19 December 2005

Abstract

The synthesis, structure, and physical properties of five R-type Ru ferrites with chemical formula $BaMRu_5O_{11}$ (M = Li and Cu) and $BaM'_2Ru_4O_{11}$ (M' = Mn, Fe and Co) are reported. All the ferrites crystallize in space group $P6_3/mmc$ and consist of layers of edge sharing octahedra interconnected by pairs of face sharing octahedra and isolated trigonal bipyramids. For M = Li and Cu, the ferrites are paramagnetic metals with the M atoms found on the trigonal bipyramid sites exclusively. For M' = Mn, Fe and Co, the ferrites are soft ferromagnetic metals. For M' = Mn, the Mn atoms are mixed randomly with Ru atoms on different sites. The magnetic structure for $BaMn_2Ru_4O_{11}$ is reported.

Keywords: R-type ferrite; $BaMRu_5O_{11}$ (M = Li; Cu); $BaM_2Ru_4O_{11}$ (M = Mn; Fe; Co); Kagome lattice

1. Introduction

Ruthenates have attracted the interest of the solid-state community because they exhibit borderline behavior between localized and itinerant electronic states that are extremely sensitive to crystal structure, dimensionality, and band filling. This leads to the manifestation of a wide spectrum of physical properties: in the Ruddlesden–Popper phases, for example, $SrRuO_3$ is an itinerant 4d ferromagnet [1], Sr_2RuO_4 is an unconventional superconductor with a T_c of 0.93 K [2], and $Sr_3Ru_2O_7$ is metamagnetic [3].

Another structural family that may give rise to interesting physical properties is the ferrites. The ferrites belong to a vast family of compounds with hexagonal and rhombohedral symmetry, which form in the systems $AO/M'O/M_2O_3$ where A = alkaline earth ion, usually Ba^{2+}; M' = metal ion such as Mg, Fe, Co, Ni or Cu; and M is a transition metal, frequently but not necessarily Fe. Ferrites such as $BaFe_{12}O_{19}$ are widely used for their insulating ferromagnetic properties. Only one ternary Ru ferrite, $BaFe_2Ru_4O_{11}$, has been reported [4]. It has the "R-type ferrite" structure type (Fig. 1), hexagonal, space group $P6_3/mmc$, consisting of edge sharing $M(2)O_6$ octahedra interconnected by face sharing $M(1)O_6$ octahedra and $M(3)O_5$ trigonal bipyramids in the ratio 2:3:1. The $M(2)O_6$ octahedra share edges such that the M ions form a Kagomé lattice in the ab plane, suggesting the possibility of geometrical frustration at low temperatures. Dimers of $M(1)O_6$ octahedra share faces perpendicular to the c-axis, which is favorable for direct M–M orbital overlap. In $BaFe_2Ru_4O_{11}$, previous work indicates that there is mixing of Fe and Ru on the $M(1)$ and $M(2)$ sites, whereas the isolated trigonal pyramidal $M(3)$ site is predominantly Fe [4].

Other transition metal R-type ferrites known are $BaTi_2Fe_4O_{11}$ [5], $BaSn_2Fe_4O_{11}$ [6] and MV_6O_{11} where M = Na [7], Sr [8] or Pb [9]. In particular, NaV_6O_{11} is

*Corresponding author. Fax: +1 416 978 8775.
E-mail address: mfoo@princeton.edu (M.L. Foo).
[1]Current address: Materials Chemistry Group, Department of Chemistry, University of Toronto, Ontario, Canada M5S 3H6.
[2]Current address: Medical Scientist Training Program and Department of Medicine, Washington University in St. Louis, 660 S. Euclid Ave., St. Louis, MO 63110, USA.

0022-4596/$ - see front matter © 2005 Elsevier Inc. All rights reserved.
doi:10.1016/j.jssc.2005.11.014

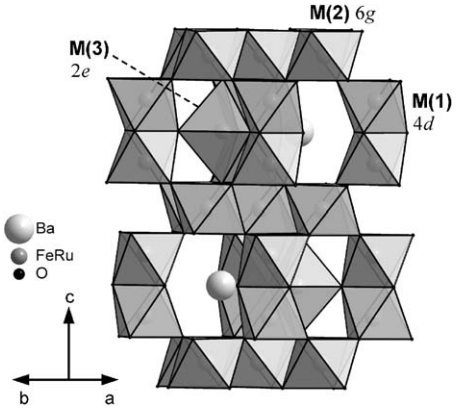

Fig. 1. The crystal structure of $BaFe_2Ru_4O_{11}$ with emphasis on the transition metal–oxygen polyhedra. The different site symmetries of the transition metal atoms are also indicated.

known for its temperature-induced structural transformations and its physical properties [10]. For these materials, only atoms with oxidation states of +3 and +4 have been reported to occupy the $M(1)$, $M(2)$ and $M(3)$ sites [11]. This suggests that the family of R-type ferrites might be extended if atoms of other oxidation states can be substituted.

As the structure of Ru ferrites suggests the possibility of geometrical magnetic frustration, metallic conductivity, and ferromagnetism, a careful study of their structure, electronic, and magnetic properties is warranted. Little is known about the physical properties of $BaFe_2Ru_4O_{11}$ [4], and there is no R-type ferrite known in the Ba–Ru–O chemical system. Here we describe the synthesis of five ternary Ba–Ru ferrites stabilized by the inclusion of ternary metals of varying electron counts, such as Li, Mn, Co, Fe and Cu. Only the Fe variant has been previously reported. The magnetic and electrical properties of these compounds were characterized from 300 to 2 K. The crystal structures of three Ba–Ru–M–O ferrites, with M = Li, Mn and Cu, were studied by neutron diffraction at 295 K. For the Mn compound, which exhibits ferromagnetic ordering, additional data were collected below its T_c, at 100 and 3.6 K. In our synthetic exploration, $BaMn_2Ru_4O_{12}$, isostructural to $BaRu_6O_{12}$ [12], was discovered. This 1-D hollandite exhibits significantly different magnetic properties than does its 3-D ferrite counterpart $BaMn_2Ru_4O_{11}$.

2. Experimental

Stoichiometric amounts of $BaCO_3$ (Alfa-Aesar 99.9%), pre-dried RuO_2 (Cerac 99.9%) and either Fe_2O_3 (Alfa-Aesar 99.99%), Co_3O_4 (Alfa-Aesar 99.7%), CuO (Alfa-Aesar 99.7%), Mn_2O_3 (Cerac 99.9%) or Li_2CO_3 (Alfa-Aesar 99%) were ground in an agate mortar and pressed into $\frac{1}{4}$in pellets. For $BaFe_2Ru_4O_{11}$ and $BaCo_2Ru_4O_{11}$, the pellets were heated at 1050 °C for 16 h. Further heating at 1100 °C for 16 h was needed for $BaLiRu_5O_{11}$ and $BaCuRu_5O_{11}$. For $BaMn_2Ru_4O_{11}$, the synthetic conditions were 1100 °C for 16 h, and 1130 °C for 16 h followed by annealing at 1125 °C for 6 h. The atmosphere in all cases was Zr-gettered nitrogen. Sample purity was checked by powder X-ray diffraction using Cu K_α radiation with variable divergence slits. A 2θ step size of 0.02° with 3.2 s dwell time was employed. Magnetic susceptibility and magnetization studies were performed from 2 to 300 K using a commercial SQUID magnetometer (Quantum Design) in fields between 100 Oe and 5 T. Resistivity measurements were made using a standard a.c. four-probe technique on pellets cut into dimensions of approximately $1.5 \times 0.5 \times 0.15$ mm.

The neutron powder diffraction (NPD) intensity data for $BaLiRu_5O_{11}$, $BaCuRu_5O_{11}$, and $BaMn_2Ru_4O_{11}$ were collected using the BT-1 high-resolution powder diffractometer at the NIST Center for Neutron Research, employing Cu (311) and Ge (311) monochromators to produce a monochromatic neutron beam of wavelengths 1.5403 and 2.0785 Å. Collimators with horizontal divergences of 15′, 20′, and 7′ full-width at half-maximum (FWHM) were used before and after the monochromator, and after the sample, respectively. The intensities were measured in steps of 0.05° in the 2θ range 3–168°. Data were collected at 295 K for $BaLiRu_5O_{11}$ and $BaCuRu_5O_{11}$. In order to study the magnetic structure, NPD data were collected at 300, 220, 100, and 3.6 K for $BaMn_2Ru_4O_{11}$. The structural parameters were refined using the program GSAS [13]. The neutron scattering amplitudes used in the refinements were 0.525, −0.203, 0.772, −0.373, 0.721, and 0.581 ($\times 10^{-12}$ cm) for Ba, Li, Cu, Mn, Ru, and O, respectively. The magnetic structure data for $BaMn_2Ru_4O_{11}$ were taken on BT-2 with pyrolytic graphite monochromator and filter, using a wavelength of 2.359 Å and collimation of 60′–42′–41′–open (FWHM). No energy analyzer was employed.

3. Results and discussion

The syntheses of phase pure ruthenium ferrites are very sensitive to preparation conditions, including time, temperature, and starting material. It was observed that for all ferrites, prolonged annealing of the pure compound in nitrogen at its original synthetic temperature invariably leads to partial decomposition and formation of Ru metal and other impurities. It was not possible to synthesize phase pure samples of $BaLiRu_5O_{11}$ without Li_2RuO_3 and RuO_2 impurities. Similarly for $BaCuRu_5O_{11}$, the product could not be obtained free from $BaRuO_3$ and Cu_2O impurities. The precise stiochiometry of these phases could only be determined by Rietveld refinement.

For $BaMn_2Ru_4O_{11}$, the temperature range for formation of the pure product is narrow due to the presence of a competing phase, the 1-D hollandite $BaMn_2Ru_4O_{12}$ (Fig. 2). This previously unknown compound is determined to be Mn-doped $BaRu_6O_{12}$ [12] from X-ray diffraction. Considering the fact that the tetragonal hollandite $BaMn_8O_{16}$ [14] is known, it is probable that Mn would

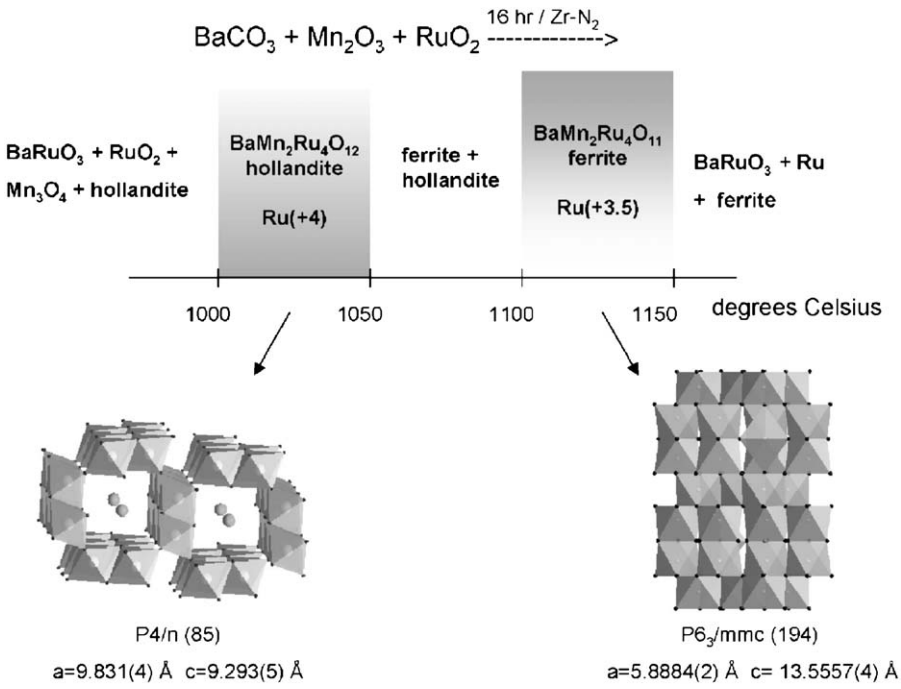

Fig. 2. The variation in structure type of Ba–Mn–Ru oxide with temperature. All samples were heated for 16 h in an atmosphere of Zr-gettered nitrogen.

substitute for Ru in a solid solution, although no attempts were made to ascertain phase boundaries. No intermediate hollandite phase could be observed for the rest of the ferrites. $BaMn_2Ru_4O_{12}$ could be converted to the ferrite $BaMn_2Ru_4O_{11}$ on increasing the annealing temperature in nitrogen. The higher annealing temperature needed to stabilize the ferrite rather than the hollandite phase is consistent with the lower average oxidation state for the transition metals in the ferrite determined by the metal-to-oxygen ratio.

The lattice parameters of the ferrites obtained by X-ray and neutron diffraction are shown in Table 1. Lattice parameters in the X-ray pattern refinements were obtained by least-squares fits to the positions of 17 peaks between 10° and 60° 2θ. The parameters derived from neutron diffraction are from Rietveld refinements.

The temperature-dependent resistivities of polycrystalline pellets of $BaLiRu_5O_{11}$, $BaFe_2Ru_4O_{11}$, $BaCo_2Ru_4O_{11}$, $BaMn_2Ru_4O_{11}$ and $BaCuRu_5O_{11}$ are shown in Fig. 3. All resistivities fall between 0.5 and 4 mΩ cm. The Co, Cu, and Mn variants show little variation of resisitivity with temperature, a characteristic, considering also the magnitude of their resisitivities, which indicates them to be poor metals. The Li variant shows a temperature-dependent resistivity that indicates that it is a good metal, though the magnitude of the resisitivity is relatively high. The Fe variant increases in resisitivity on decreasing temperature, but both the magnitude of the resisitivity and its increase on cooling are too small to be indicative of truly semiconducting behavior. Thus it is also likely a poor metal, with the increasing resisitivity in the polycrystalline pellet likely due to the presence of grain boundary effects. In Fig. 4, the resistivity of $BaMn_2Ru_4O_{11}$ ferrite and

Table 1
Lattice parameters of ruthenium ferrites $BaM_2Ru_4O_{11}$ (M = Fe, Co, Mn) and $BaM'Ru_5O_{11}$ (M' = Li, Cu) determined by powder X-ray diffraction (represented by *) or neutron powder diffraction (represented by **)

	a/Å	c/Å
$BaFe_2Ru_4O_{11}$	5.895(2)	13.483(3)*
$BaCo_2Ru_4O_{11}$	5.851(3)	13.483(6)*
$BaMn_2Ru_4O_{11}$	5.8884(2)	13.5557(4)**
$BaLiRu_5O_{11}$	5.8114(2)	13.7895(5)**
$BaCuRu_5O_{11}$	5.8445(2)	13.8099(4)**

Space group: $P6_3/mmc$ (No. 194).

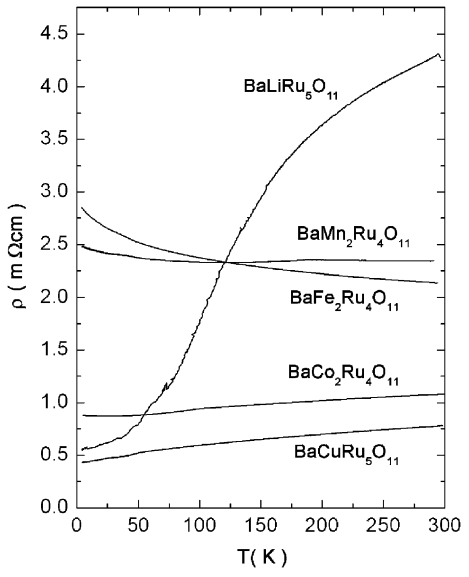

Fig. 3. Temperature-dependent resistivity of ruthenium ferrites $BaLiRu_5O_{11}$, $BaFe_2Ru_4O_{11}$, $BaMn_2Ru_4O_{11}$, $BaCo_2Ru_4O_{11}$ and $BaCuRu_5O_{11}$.

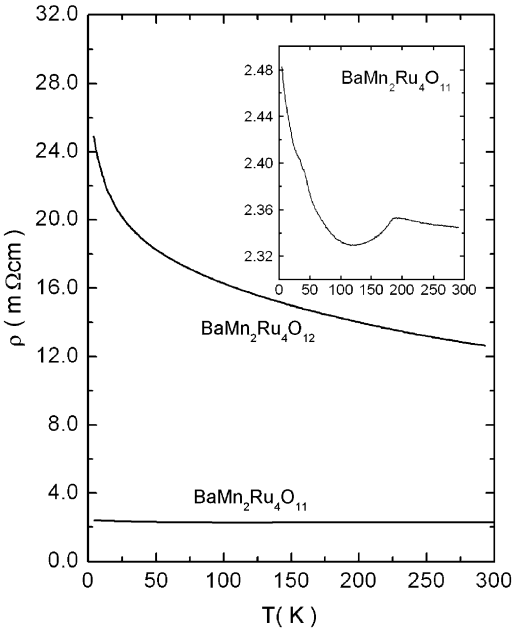

Fig. 4. Temperature-dependent resistivity of $BaMn_2Ru_4O_{11}$ ferrite and $BaMn_2Ru_4O_{12}$ hollandite. Inset: resistivity of $BaMn_2Ru_4O_{11}$ emphasizing the weak transition at 175 K.

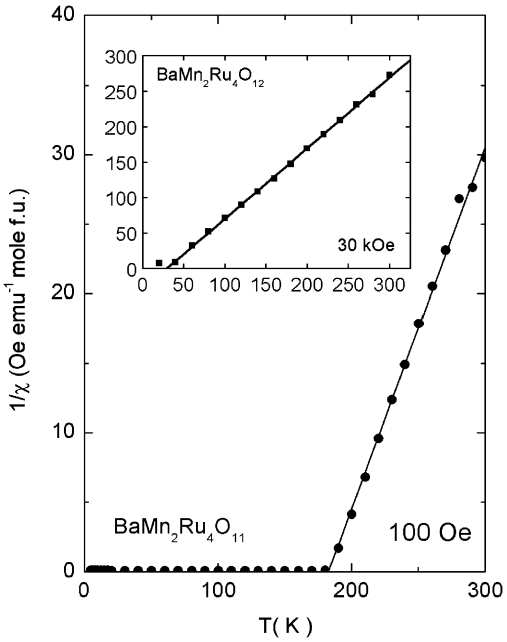

Fig. 6. $1/\chi$ vs. T plot for $BaMn_2Ru_4O_{11}$ ferrite with $\theta_{CW} = 185$ K. Inset: $1/\chi$ vs. T plot for $BaMn_2Ru_4O_{12}$ hollandite with $\theta_{CW} = 30$ K.

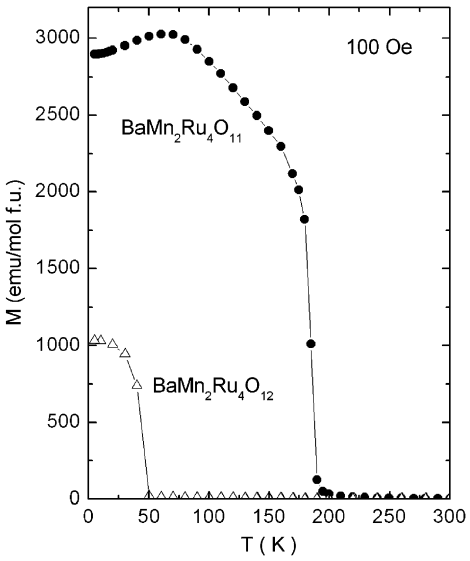

Fig. 5. Field cooled magnetic susceptibility of $BaMn_2Ru_4O_{11}$ ferrite and $BaMn_2Ru_4O_{12}$ hollandite (100 Oe).

$BaMn_2Ru_4O_{12}$ hollandite are compared, showing that $BaMn_2Ru_4O_{12}$ is also a poor metal. The inset of Fig. 4 shows that a kink is seen in the resistivity for $BaMn_2Ru_4O_{11}$ at 175 K. This occurs at the magnetic ordering temperature (see below). There is also a small kink in the resisitivity of $BaCo_2Ru_4O_{11}$ (Fig. 3) at 100 K, the temperature of its ferromagnetic ordering transition (see below).

The field cooled magnetic susceptibilities of $BaMn_2Ru_4O_{11}$ and $BaMn_2Ru_4O_{12}$, measured in a 100 Oe field, are shown in Fig. 5. Both compounds are ferromagnetic, with ordering temperatures at 200 and 50 K, respectively. The $1/\chi$ vs. T plot for $BaMn_2Ru_4O_{11}$ indicates that θ_{CW} is 185 K (Fig. 6). Due to the presence of trace amounts of ferrite impurities, the $1/\chi$ vs. T plot for $BaMn_2Ru_4O_{12}$ was measured at a higher field, 30 kOe, giving $\theta_{CW} = 30$ K. The M–H loops from -5 to 5 T at 5 K for both compounds are shown in Fig. 7. It clearly shows the hollandite has a higher coercive field but a lower saturation magnetization compared to its ferrite counterpart. As undoped $BaRu_6O_{12}$ hollandite is paramagnetic [15], it would be interesting to determine whether the observed ferromagnetism in $BaMn_2Ru_4O_{12}$ can be attributed to ordering of Mn spins alone or to both Mn and Ru spins. On decreasing the doping of Mn to $BaMn_{0.5}Ru_{5.5}O_{12}$, no ferromagnetic behavior was observed, indicating that the ferromagnetism observed in $BaMn_{2-x}Ru_{4+x}O_{12}$ appears between $x = 0$ and 1.5.

For $BaCo_2Ru_4O_{11}$, the high-temperature magnetic susceptibility (Fig. 8) can be fitted to a Curie–Weiss law after the subtraction of a temperature-independent term (0.04 emu Oe^{-1} mol^{-1} f.u.), yielding $\theta_{CW} = 111$ K and a moment of 6.42 μ_B per formula unit. M–H loops taken at 10 and 73 K (Fig. 9) confirm ferromagnetic ordering with a low coercive field of approximately 250 Oe.

For $BaFe_2Ru_4O_{11}$, the magnetic ordering temperature was above room temperature and therefore no attempt was made to determine T_c. Field-dependent magnetization measurements at 10 K (Fig. 10) show that the ferromagnetic part of the magnetization grows between 235 and 10 K. The fact that the magnetization does not appear to be fully saturated by 3 T at 10 K suggests that measurements at higher fields may be of interest. For $BaLiRu_5O_{11}$ (Fig. 11), temperature-independent paramagnetism is

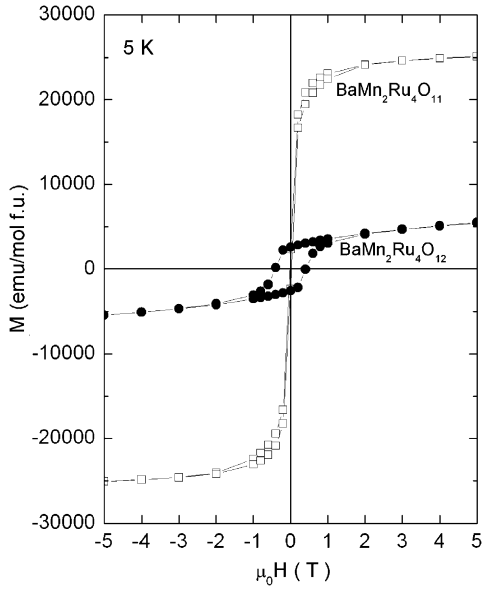

Fig. 7. *M–H* loops of $BaMn_2Ru_4O_{11}$ and $BaMn_2Ru_4O_{12}$ from −5 to 5 T at 5 K.

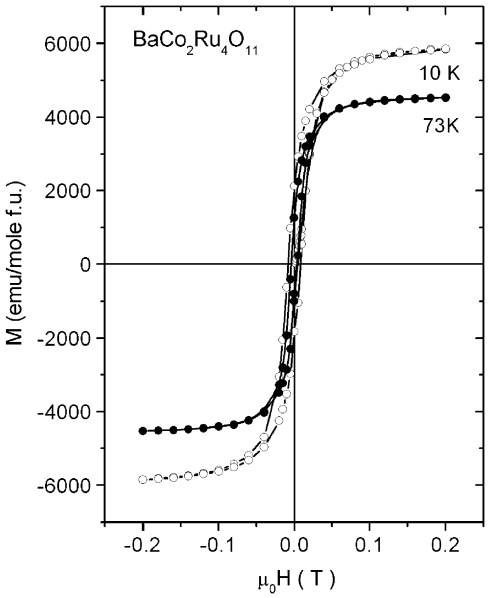

Fig. 9. *M–H* loops for $BaCo_2Ru_4O_{11}$ from −0.2 to 0.2 T at 10 and 73 K.

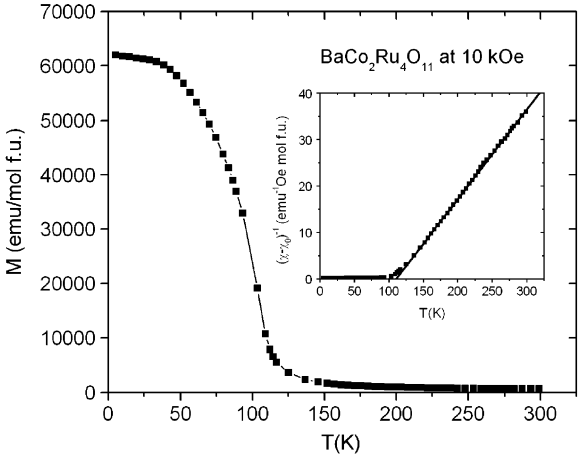

Fig. 8. Temperature-dependent magnetic susceptibility for $BaCo_2Ru_4O_{11}$ at 10 kOe under zero field cooling. Inset: $1/(\chi-\chi_o)$ vs. T plot with $\theta_{CW} = 111$ K, $\mu = 6.4\,\mu_B$ per f.u.

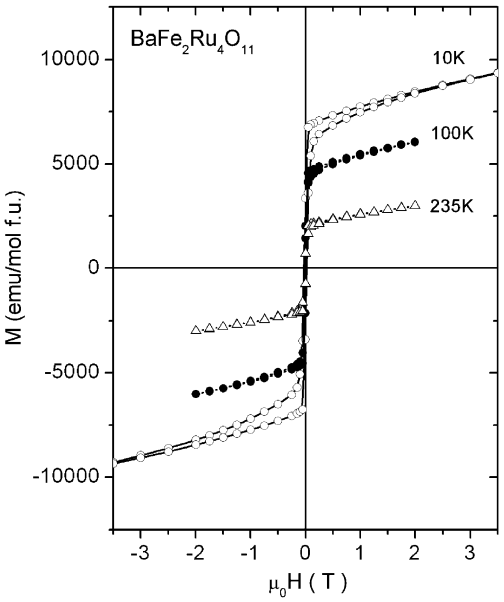

Fig. 10. *M–H* loops for $BaFe_2Ru_4O_{11}$ from −3.5 to 3.5 T at 10, 100 and 235 K.

observed, with the contribution of a very small number of paramagnetic impurities at low temperature. No local moment on Ru is induced when Li, a non-magnetic atom with no *d* electrons, is present in the ferrite structure. This is in contrast to what is observed in $CaRuO_3$, for example, where ferromagnetism was induced with 5% doping of non-magnetic Ti [16] on the Ru site. For $BaCuRu_5O_{11}$, a similar temperature-independent contribution to the susceptibility is observed, but there is an additional contribution of some local moment leading to an increase in susceptibility by a factor of three on cooling from room temperature to 5 K. The origin of this localized moment cannot be strictly determined at this time, but may be of future interest.

3.1. Neutron diffraction

To increase our understanding of the structure–property relationships in the Ru ferrites, three ferrites, $BaLiRu_5O_{11}$, $BaCuRu_5O_{11}$ and $BaMn_2Ru_4O_{11}$ were selected for neutron diffraction. Additional measurements were carried out on $BaMn_2Ru_4O_{11}$, at 3.6 and 100 K to probe for long-range magnetic order.

Due to their structural similarities and lack of magnetic ordering, $BaLiRu_5O_{11}$ and $BaCuRu_5O_{11}$ will be discussed first. The initial structural model, in space group $P6_3/mmc$,

was taken from $BaFe_2Ru_4O_{11}$ [4]. In the initial models, the Li (or Cu) and Ru atoms were mixed and occupy 2*d*, 4*e*, and 6*g* sites and the occupancy parameters of Li (or Cu) and Ru at each site were refined, being constrained to be consistent with the chemical and structural formula n(Li (or Cu))$+n$(Ru) = 1. Results indicate that the Li and Cu occupy the 2*d* site for $BaLiRu_5O_{11}$ and $BaCuRu_5O_{11}$. The refined percentage of Ru at the 2*d* site was found to be within two standard deviations of zero, and was then set to zero in the final refinement. Refined percentages of Li (or Cu) on the 4*e* and 6*g* sites in $BaLiRu_5O_{11}$ (or $BaCuRu_5O_{11}$) were also found to be within two standard deviations of zero and were also fixed to be zero in the final refinements. Impurity phases of RuO_2 (2.9(1)%) and Li_2RuO_3 (3.9(2)%) were found in the $BaLiRu_5O_{11}$ sample and Cu_2O (4.0(1)%) and 9R $BaRuO_3$ (4.0(3) %) were found in the $BaCuRu_5O_{11}$ sample, and were taken into account in final refinements. Table 2 presents the refined structural parameters for $BaLiRu_5O_{11}$ and $BaCuRu_5O_{11}$ at room temperature.

For the structure determination of $BaMn_2Ru_4O_{11}$ (Fig. 12), the same initial structure model was used and

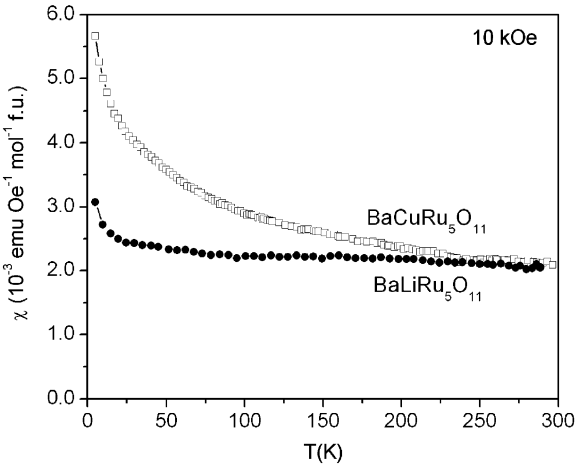

Fig. 11. Temperature-dependent magnetic susceptibility for $BaCuRu_5O_{11}$ and $BaLiRu_5O_{11}$ at 10 kOe under zero field cooling.

Table 2
Structural parameters of $BaMRu_5O_{11}$, (M = Li and Cu) at 295 K

Atom	Parameter	$BaLiRu_5O_{11}$	$BaCuRu_5O_{11}$
	a (Å)	5.8114(2)	5.8445(2)
	c (Å)	13.7895(5)	13.8099(4)
	V (Å^3)	403.31(3)	408.525
Ba	B (Å^2)	0.7(2)	0.7(1)
M	B (Å^2)	2.8(6)	1.2(6)
Ru(1)	z	0.1575(3)	0.1530(3)
	B (Å^2)	0.62(7)	0.47(1)
Ru(2)	B (Å^2)	1.36(6)	1.40(6)
O(1)	x	0.1693(3)	0.1703(3)
	z	0.0802(3)	0.0797(2)
	B (Å^2)	0.88(6)	0.96(5)
O(2)	x	0.8524(4)	0.8542(3)
	B (Å^2)	0.24(7)	0.29(6)
O(3)	z	0.5808(6)	0.5785(5)
	B (Å^2)	2.6(2)	2.4(2)
	R_p(%)	6.58	5.65
	R_{wp} (%)	8.37	7.39
	χ^2	2.923	2.708

Space group: $P6_3/mmc$. M and Ru occupy three independent crystallographic sites: M, 2*d* (1/3, 2/3, 3/4); Ru(1), 4*e* (0 0 *z*), Ru(2), 6*g* (1/2, 0, 0); Ba is at 2*b* (0, 0, 1/4) site; O(1), O(2), and O(3) are at 12*k* (*x*, 2*x*, *z*), 6*h* (*x*, 2*x*,1/4), and 4*f*(1/3, 2/3, *z*), respectively.
Impurity phases RuO_2 and Li_2RuO_3 found in the $BaLiRu_5O_{11}$ sample are 2.9(1)% and 3.9(2)%, respectively.
Impurity phases Cu_2O and 9R $BaRuO_3$ found in the $BaCuRu_5O_{11}$ sample are 4.0(1)% and 4.0(3)%, respectively.

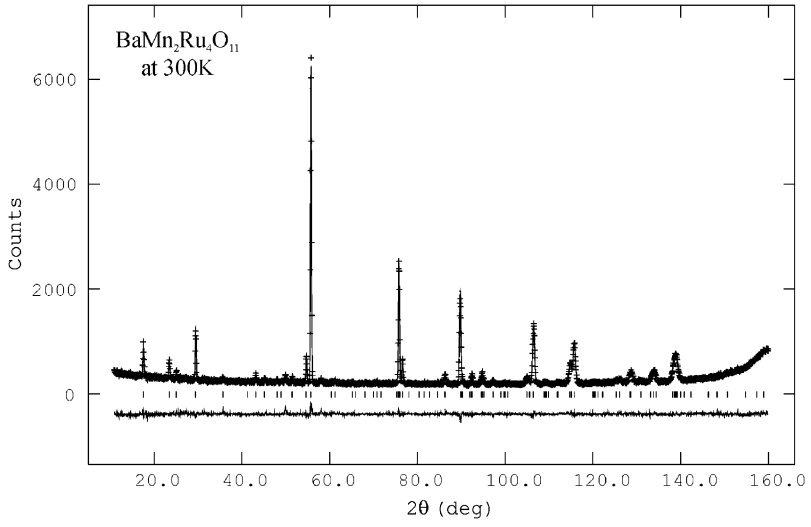

Fig. 12. Observed (crosses) and calculated (solid curve) NPD intensities of $BaMn_2Ru_4O_{11}$ at 300 K. Vertical lines show the Bragg peak positions for $BaMn_2Ru_4O_{11}$. Differences are shown at the bottom of the figure.

Table 3
Structural parameters of $BaMn_2Ru_4O_{11}$

Atom	Parameter	3.6 K	100 K	220 K	300 K
	a (Å)	5.8808(2)	5.8808(2)	5.8839(2)	5.8884(2)
	c (Å)	13.5313(4)	13.5330(4)	13.5439(4)	13.5557(4)
	V (Å^3)	405.27(3)	405.32(3)	406.7(3)	407.04(3)
Ba	B (Å^2)	0.68(2)	1.5(2)	1.3(2)	0.8(1)
Mn/Ru(1)	z	0.1500(3)	0.1487(4)	0.1495(4)	0.1507(3)
	B (Å^2)	0.90(6)	1.04(9)	1.01(9)	0.80(5)
	n(Mn)	0.152(5)	0.176(9)	0.164(9)	0.175(5)
Mn/Ru(2)	B (Å^2)	0.90(6)	1.04(9)	1.01(9)	0.80(6)
	n(Mn)	0.228(4)	0.220(6)	0.231(6)	0.241(4)
	M_x(Mn) μ_B	−1.24(8)	−1.4(1)	0	0
	M_y(Mn) μ_B	−2.48(16)	−2.9(2)	0	0
	M_z(Mn) μ_B	1.8(3)	0	0	0
	M(Mn) μ_B	3.3(2)	3.2(3)	0	0
Mn/Ru(3)	B (Å^2)	0.90(6)	1.04(9)	1.01(9)	0.80(6)
	n(Mn)	0.980(6)	0.987(9)	0.965(9)	0.959(6)
	M_x(Mn) μ_B	0	0	0	0
	M_y(Mn) μ_B	0	0	0	0
	M_z(Mn) μ_B	3.59(7)	2.7(1)	0	0
	M(Mn) μ_B	3.59(7)	2.7(1)	0	0
O(1)	x	0.1713(2)	0.1708(3)	0.1705(3)	0.1714(2)
	z	0.0798(2)	0.0805(3)	0.0804(3)	0.0801(2)
	B (Å^2)	0.74(4)	1.12(8)	1.11(8)	1.20(5)
O(2)	x	0.8547(3)	0.8538(4)	0.8545(4)	0.8547(3)
	B (Å^2)	0.35(6)	0.4(1)	0.5(1)	0.80(6)
O(3)	z	0.5810(4)	0.5818(6)	0.5810(5)	0.5815(4)
	B (Å^2)	1.7(1)	1.5(2)	1.6(2)	1.6(1)
	Refined $\sum$n(Mn)	**1.97(1)**	**2.00(1)**	**1.99(1)**	**2.03(1)**
	R_p(%)	4.61	4.62	4.97	5.17
	R_{wp} (%)	5.80	5.79	6.05	6.46
	χ^2	1.109	1.099	1.104	0.9638

Space group: $P6_3/mmc$ (No. 194). Mn and Ru occupy three independent crystallographic sites: Mn/Ru(1), 4*e* (00*z*); Mn/Ru(2), 6*g* (1/2,0,0); and Mn/Ru(3), 2*d* (1/3,2/3,3/4). Ba is at 2*b* (0,0,1/4) site, O(1), O(2), and O(3) are at 12*k* (*x*,2*x*,*z*), 6*h* (*x*,2*x*,1/4), and 4*f*(1/3,2/3,*z*), respectively. The magnetic structure has the symmetry of Shubnikov group $P6_3/mm'c'$ (No. 270).
The occupancy parameters *n* for 2*d*, 4*e*, and 6*g* sites were constrained to be n(Mn) + n(Ru) = 1.

the same refinement procedures were performed. Refinements showed that the Mn and Ru atoms are mixed, and randomly occupy the 2*d*, 4*e*, and 6*g* sites, with occupancies n(Mn) at 300 K of 0.959(6), 0.175(5), and 0.241(4), respectively. Values very close to these were obtained from all the data sets at different temperatures, and all of these are in very good agreement with the nominal composition $BaMn_2Ru_4O_{11}$ (Table 3). No nuclear structural transition was found between 3.6 and 300 K. This is in contrast to NaV_6O_{11}, which undergoes two structural transformations in the same temperature range [17]. The observed and calculated intensities and structural parameters at 300 K for $BaMn_2Ru_4O_{11}$ are shown in Fig. 12 and Table 3, respectively.

3.2. Crystal structure

Table 4 shows selected interatomic distances and angles determined in the neutron diffraction refinements for $BaLiRu_5O_{11}$, $BaCuRu_5O_{11}$ and $BaMn_2Ru_4O_{11}$ at room temperature. The metal atoms Ru/Mn(1) or Ru/Mn(2) at the 4*e* or 6*g* sites have octahedral coordination by six oxygen atoms (Fig. 1). The 6*g*-site octahedra are edge sharing in the *ab* plane. Two 4*e*-site octahedra are connected by face sharing and the corners share with the 6*g*-site octahedra directly above and below along the *c*-axis. The metal atom (Li, Cu or Mn/Ru) in the 2*d* site is surrounded by five oxygen atoms, forming a trigonal bipyramid with three short in-plane bond distances (~1.9 Å) and two longer apical distances (~2.3 Å). Due to the unique coordination of the trigonal pyramidal site, the valences calculated for M = Li and Cu are atypical. For the edge sharing 6*g* sites, the Ru valence is +3.80 for M = Li and +3.82 for M = Cu, suggesting that the Kagome layers are rather conductive. Ru valences calculated for the face sharing 4*e* sites are +4 for M = Li and +3.94 for M = Cu, similar to 4H $BaRuO_3$

Table 4
Selected interatomic distances (Å) and angles (deg) of $BaLiRu_5O_{11}$ (295 K), $BaCuRu_5O_{11}$ (295 K) and $BaMn_2Ru_4O_{11}$ (300 K)

	$BaLiRu_5O_{11}$	$BaCuRu_5O_{11}$	$BaMn_2Ru_4O_{11}$
Ba–O(1) × 6	2.865(3)	2.874(3)	2.8349(3)
Ba–O(2) × 6	2.9121(3)	2.9299(3)	2.9522(2)
2d site $M(3)O_5$ elongated double triangle pyramid (M = Li or Cu or Mn/Ru)			
$M(3)$–O(2) × 3	1.870(4)	1.898(3)	1.918(3)
$M(3)$–O(3) × 2	2.333(8)	2.368(6)	2.2845(5)
$M(3)$–$M(1)$	3.590(1)	3.631(1)	3.657(1)
$M(3)$–$M(2)$	3.8339(1)	3.8427(1)	3.7913(1)
Valence V_M (e.u.)	**1.20**	**1.58**	
O(2)–$M(3)$–O(2)	120	120	120
O(2)–$M(3)$–O(3)	90	90	90
O(3)–$M(3)$–O(3)	180	180	180
4e site $M(1)O_6$ face sharing octahedron (M = Ru or Mn/Ru)			
$M(1)$–O(1) × 3	2.013(3)	2.033(3)	1.993(3)
$M(1)$–O(2) × 3	1.954(3)	1.951(3)	2.002(3)
$M(1)$–$M(1)$	2.552(8)	2.680(7)	2.693(8)
$M(1)$–$M(2)$	3.627(2)	3.606(2)	3.583(2)
Valence $V_{Ru(1)}$ (e.u.)	**4.02**	**3.94**	
O(1)–$M(1)$–O(1)	94.3(1)	94.5(1)	98.9(2)
O(1)–$M(1)$–O(2)	171.6(1)	171.2(1)	166.4(2)
O(1)–$M(1)$–O(2)	91.39(9)	91.46(8)	89.8(8)
O(2)–$M(1)$–O(2)	82.3(1)	81.9(1)	79.7(2)
6g-site $M(2)O_6$ edge sharing octahedron (M = Ru or Mn/Ru)			
$M(2)$–O(1) × 4	1.998(3)	1.999(2)	1.997(2)
$M(2)$–O(3) × 2	2.014(5)	2.005(3)	2.027(3)
$M(2)$–$M(2)$	2.90572(9)	2.92227(9)	2.99418(9)
Valence $V_{Ru(2)}$ (e.u.)	**3.80**	**3.82**	
O(1)–$M(2)$–O(1)	91.4(2)	91.3(2)	91.5(2)
O(1)–$M(2)$–O(1)	180	180	180
O(1)–$M(2)$–O(1)	88.6(2)	88.7(2)	88.5(2)
O(1)–$M(2)$–O(3)	92.8(2)	93.7(1)	94.0(1)
O(1)–$M(2)$–O(3)	87.2(2)	86.3(1)	86.0(1)
O(3)–$M(2)$–O(3)	180	180	180

The bond valence sum, V in electron units (e.u.) is given by $\sum_j \exp[(R_{ij}-d_{ij})/b]$, where the d_{ij} is the bond distance, $b = 0.37$, and R_{ij} are 1.466, 1.593, and 1.834 for Li^+, Cu^+, and Ru^{4+} ions, respectively [18].

with face sharing Ru_2O_9 dimers [19]. In M = Li, the Ru–Ru distance in the $M(1)$ site is 2.55 Å, which is significantly shorter than the closest distance in Ru metal (2.65 Å), but almost equivalent to the bond distance of the Ru_2O_9 dimer in 4H $BaRuO_3$ (2.54 Å) [19]. This suggests that similar to $BaRuO_3$, there is significant Ru–Ru bonding in $BaLiRu_5O_{11}$. For M = Cu this distance is 2.68 Å, suggesting that there is probably no significant Ru–Ru bonding.

3.3. Magnetic structure of $BaMn_2Ru_4O_{11}$

Magnetic intensities were observed in the data at 100 and 3.6 K (Fig. 13) for $BaMn_2Ru_4O_{11}$. The inset to Fig. 13 shows the observed and calculated nuclear structure neutron powder pattern in the lower angle regime where magnetic peaks are expected. The magnetic peaks superpose on the nuclear peaks, indicating that the magnetic structure has the same cell dimensions as the nuclear structure. A magnetic structure model with symmetry of Shubnikov group $P6_3/mm'c'$ (No. 270) [20] gave a good fit to the magnetic intensities (Table 3). In this magnetic structure model, symmetry allows only a c component M_z for the magnetic atoms located at the 2d and 4e sites, while those at the 6g site may have both in-plane components, related by M_x, $M_y = 2M_x$, and a c component M_z. Due to the low moments expected for Ru^{4+} and Ru^{3+} ions and the sharply decreasing angular dependence of the magnetic form factor, we conclude that the magnetic intensities are dominated by the ordered magnetic moments of Mn^{3+} ions, and therefore only refined moments based on the Mn^{3+} form factor. The results indicate that there is no ordered moment detected on the 4e site (which has the smallest Mn content) at any temperature. The 2d site, on the other hand, orders ferromagnetically with the moments parallel to the c-axis and values of 3.59(7) and 2.7(1) μ_B at 3.6 and 100 K, respectively. For the interesting 6g sites, which form a Kagomé structure in the ab plane, we find a 120° triangular magnetic structure, characteristic of a frustrated lattice with antiferromagnetic nearest-neighbor interactions [21], as shown on the right in Fig. 14. At 100 K we obtained moments of $M_x = -1.4(1)$, $M_z = 0$, and $M = 3.2(3)\,\mu_B$. This is the simplest "$q = 0$" structure, which exhibits uniform vector chirality [22]. Other 120° magnetic structures, such as the $\sqrt{3} \times \sqrt{3}$ which has staggered vector chirality, did not fit the data.

At low temperatures we find that each plaquette of spins tilts along the c-axis, with an ordered moment of $M_x = -1.24(8)$, $M_z = 1.8(3)$, and $M = 3.3(2)\,\mu_B$ at 3.6 K. The orientation of spins on the different Mn sites for 3.6 and 100 K are shown schematically in Fig. 14. Note in particular that the net moments on both types of sites are parallel and give rise to a substantial net magnetization. The development of the net moment on the Kagomé lattice is particularly interesting because it signifies the presence of a non-zero scalar chirality. Fig. 15 shows the magnetic peak (1 0 1) intensity as a function of temperature, where we see that the intensity develops continuously below the ordering temperature. The solid curve is a mean field fit to the data to estimate the ordering temperature of 188.6(4) K. We note that this ordering temperature is in good agreement with the transition temperature in the magnetization data and the observed anomaly in the resistivity data. The continuous evolution of the magnetic order likely indicates that there is a c-axis moment on the 6g site, implying a non-zero scalar chirality, in the entire ordered phase, even though it is below our detectable limit at 100 K. Further progress in understanding the details of this interesting magnetic phase will have to await the availability of single crystals.

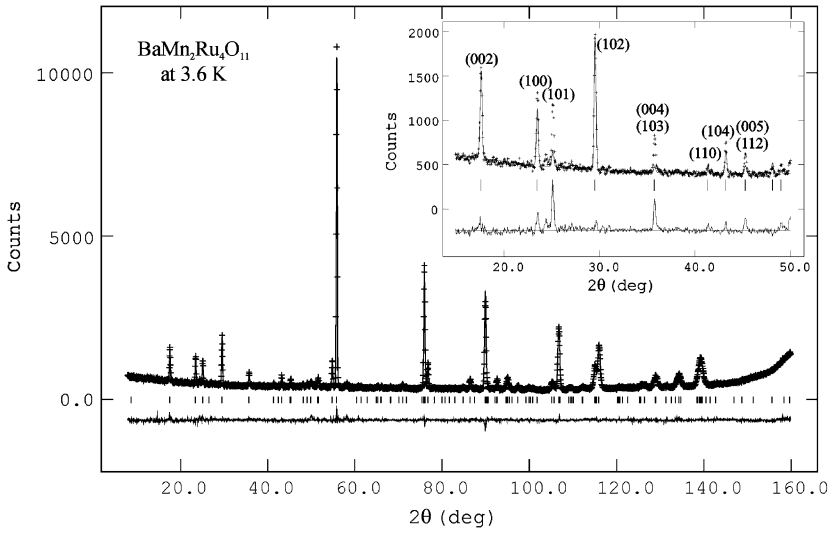

Fig. 13. Observed (crosses) and calculated (solid line) NPD intensities of $BaMn_2Ru_4O_{11}$ at 3.6 K. Vertical lines show the Bragg peak positions. Lower curve shows the difference between observed and calculated patterns. Inset shows the fit with nuclear structure only, where the magnetic peaks are clearly indicated on the difference curve.

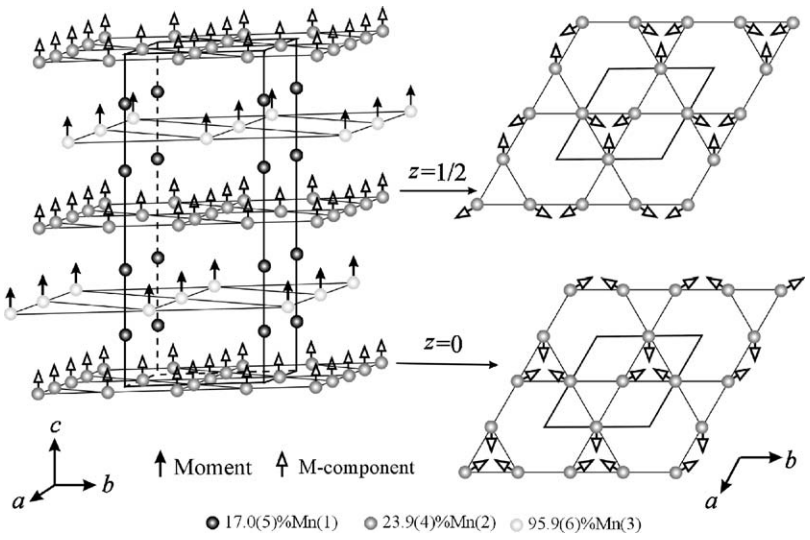

Fig. 14. Magnetic structure model used in the refinement for $BaMn_2Ru_4O_{11}$ at 3.6 and 100 K. The structure has the symmetry of Shubnikov group $P6_3/mm'c'$ (No. 270). No ordered moments were found at the 4*e* site at any temperature. The solid arrows show that the moments for atoms at the 2*d* site are parallel to the *c*-axis and form a ferromagnetic arrangement below the ordering temperature of 188 K. The open arrows show the in-plane and out-of-plane components of the moments for atoms at the 6*g* sites, which form a Kagomé lattice in the plane. At 100 K the spins exhibit the triangular 120° '$q = 0$' structure (right panel), which possesses uniform vector chirality. At 3.6 K, a substantial M_z component develops, which indicates a non-zero scalar chirality for this sublattice.

4. Conclusion

In summary, we have synthesized a series of ternary Ba–Ru ferrites with two types of chemical formula, $BaMRu_5O_{11}$ and $BaM'_2Ru_4O_{11}$ where $M = Li$, Cu and $M' = Fe$, Co, Mn. For $M' = Mn$, a new 1-D tetragonal hollandite phase, $BaMn_2Ru_4O_{12}$ was observed at a lower synthetic temperature compared to its ferrite counterpart. The electrical and magnetic properties of the ferrites were characterized. In comparison to the perovskites [23], the Ba–Ru ferrites are poor metals. $BaLiRu_5O_{11}$ and $BaCuRu_5O_{11}$ are paramagnetic, whereas $BaFe_2Ru_4O_{11}$, $BaCo_2Ru_4O_{11}$ and $BaMn_2Ru_4O_{11}$ are soft ferromagnetic materials with low coercive fields. Given the anisotropy shown in the physical properties of NaV_6O_{11} [24] and more recently, $SrCo_6O_{11}$ [25], single crystals of ternary Ba–Ru ferrites might be of interest for further study.

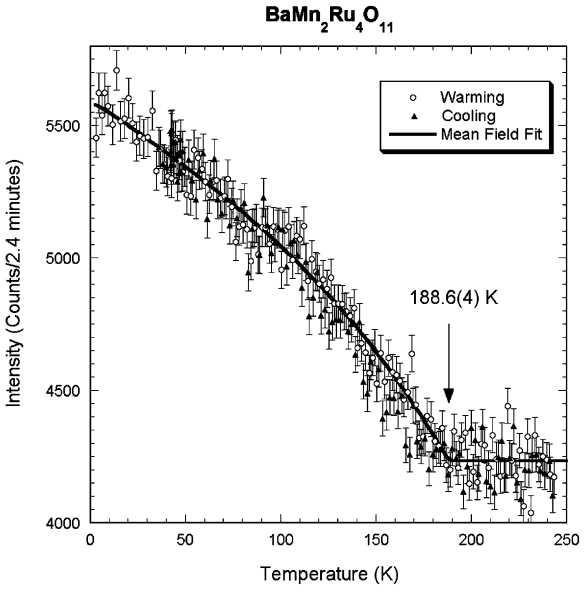

Fig. 15. Magnetic peak (1 0 1) intensity as a function of temperature for $BaMn_2Ru_4O_{11}$. The solid curve is a mean field fit to the data to estimate the ordering temperature of 188.6(4) K.

Acknowledgments

This work was supported by the US National Science Foundation, Grants DMR-0244254 and DMR-0213706.

References

[1] J.M. Longo, P.M. Raccah, J.B. Goodenough, J. Appl. Phys. 39 (2) (1968) 1327.
[2] Y. Maeno, H. Hashimoto, K. Yoshida, S. Nishizaki, T. Fujita, J.G. Bednorz, F. Lichtenberg, Nature 372 (1994) 532.
[3] S.A. Grigera, R.S. Perry, A.J. Schofield, M. Chiao, S.R. Julian, G.G. Lonzarich, S.I. Ikeda, Y. Maeno, A.J. Millis, A.P. Mackenzie, Science 294 (2001) 329.
[4] D. Verdoes, H.W. Zandbergen, D.J.W. Ijdo, Mater. Res. Bull. 22 (1987) 1.
[5] V.F. Haberey, M. Velicescu, Acta Crystallogr. B 30 (1974) 1507.
[6] M.C. Cadee, D.J.W. Ijdo, J. Solid State Chem. 52 (1984) 302.
[7] M.E. DeRoy, J.P. Besse, R. Chevalier, M. Gasperin, J. Solid State Chem. 67 (1987) 185.
[8] Y. Kanke, F. Izumi, E. Takayama-Muromachi, K. Kato, T. Kamiyama, H. Asano, J. Solid State Chem. 92 (1990) 261–272.
[9] O. Mentre, F. Abraham, J. Solid State Chem. 125 (1996) 91.
[10] H. Kato, M. Kato, K. Yoshimura, K. Kosuge, J. Phys.: Condens. Matter 13 (2001) 9311.
[11] Y. Kanke, K. Kato, E. Takayama-Muromachi, M. Isobe, Acta Crystallogr. C 48 (1992) 1376.
[12] C.C. Toradi, Mater. Res. Bull. 20 (6) (1985) 705.
[13] A. Larson, R.B. Von Dreele, Los Alamos National Laboratory, Internal Report 1994.
[14] A. Bystrom, A.M. Bystrom, Acta Crystallogr. 3 (1950) 146.
[15] Z.Q. Mao, T. He, M.M. Rosario, K.D. Nelson, D. Okuno, B. Ueland, I.G. Deac, P. Schiffer, Y. Liu, R.J. Cava, Phys. Rev. Lett. 90 (18) (2003) 186601.
[16] T. He, R.J. Cava, J. Phys.: Condens. Matter 13 (2001) 8347.
[17] Y. Kanke, F. Izumi, Y. Morii, E. Akiba, S. Funahashi, K. Kato, M. Isobe, E. Takayama-Muromachi, Y. Uchida, J. Solid State Chem. 112 (1994) 429.
[18] N.E. Brese, M. O'Keeffe, Acta Crystallogr. B 47 (1991) 192.
[19] S.T. Hong, A.W. Sleight, J. Solid State Chem. 128 (1997) 251.
[20] N.V. Belov, N.N. Neronova, T.S. Smirnova, Sov. Phys. Crystallogr. 2 (1957) 311.
[21] For a review see M.F. Collins, O.A. Petrenko, Can. J. Phys. 75 (1997) 605.
[22] D. Grohol, K. Matan, J.H. Cho, S.-H. Lee, J.W. Lynn, D.G. Nocera, Y.S. Lee, Nat. Mater. 4 (2005) 323.
[23] J.T. Rijissenbeck, Q. Huang, R.W. Erwin, H.W. Zandbergen, R.J. Cava, J. Solid State Chem. 146 (1999) 65.
[24] Y. Uchida, Y. Kanke, E. Takayama-Muromachi, K. Kato, J. Phys. Soc. Jpn. 60 (8) (1991) 2530.
[25] S. Ishiwata, D. Wang, T. Saito, M. Takano, Chem. Mater. 17 (2005) 2789.